Surface ocean cooling in the Eocene North Atlantic coincides with declining atmospheric CO_2

Gordon N. Inglis* (1), Rehemat Bhatia* (2), David Evans (1,3), Jiang Zhu(4), Wolfgang Müller (3), David Mattey (5) David Thornalley (6), Richard G. Stockey (1), Bridget S. Wade (2)

(1) School of Ocean and Earth Science, University of Southampton, UK

(2) Department of Earth Sciences, University College London, UK

(3) Institute of Geosciences, Goethe University Frankfurt, Frankfurt, Germany

(4) National Center for Atmospheric Research, Colorado, USA

(5) Department of Earth Sciences, Royal Holloway University of London (RHUL), UK

(6) Department of Geography, UCL, UK

* contributed equally to this work

Corresponding author: Gordon N. Inglis

Email: gordon.inglis@soton.ac.uk. Telephone: +44 (0)117 954 6395

Key points:

- Long-term decline in North Atlantic sea surface temperatures (~5° C) between the early (~53 Ma) and the middle (~42 Ma) Eocene.
- This indicates that CO_2 was likely responsible for the onset of long-term Eocene cooling.
- However, zonal temperature gradients in the North Atlantic appear decoupled due to inception of Northern Component Water formation.

Abstract:

The Eocene (56–34 million years ago) is characterised by declining sea surface temperatures (SSTs) in the low latitudes (~4°C) and high southern latitudes (~8-11°C), in accord with decreasing CO_2 estimates. However, in the mid-to-high northern latitudes there is no evidence for surface water cooling, suggesting thermal decoupling between northern and southern hemispheres and additional non-CO_2 controls. To explore this further, we present a multi-proxy (Mg/Ca, $\delta^{18}O$, TEX_{86}) SST record from the western North Atlantic (~36°N paleolatitude). Our data confirm a long-term decline in SSTs of ~5°C between the early (~53 Ma) and the middle (~42 Ma) Eocene, supporting declining atmospheric CO_2 as the primary mechanism of Eocene cooling. However, from the middle Eocene onwards, North Atlantic zonal temperature gradients are decoupled, which we attribute to the incursion of warmer waters into the eastern North Atlantic and the inception of Northern Component Water across the early-middle Eocene transition.

Introduction

The early Eocene Climatic Optimum (EECO; 53.3 to 49.1 million years ago; Ma) (Hollis et al., 2019a) is characterised by a long-term maximum in atmospheric CO_2 (~1470 ppm) (Anagnostou et al., 2020), followed by a gradual decline in atmospheric CO_2 during the middle Eocene (47.8 to 38.0 Ma) to ~800ppm (Anagnostou et al., 2020). This is consistent with declining SSTs in the tropics (ca. 4°C) (Cramwinckel et al., 2018; Evans et al., 2018) and the mid-to-high southern latitudes (ca. 8-11 °C; Bijl et al., 2009; Hollis et al., 2009; Hollis et al., 2012). However, SST estimates from the eastern North Atlantic suggest relatively muted surface water cooling (~1°C) between the EECO and middle Eocene (~40 Ma) (Bornemann et al., 2016). Temperature asymmetry between the northern and southern hemisphere would not be expected from a long-term decline in atmospheric CO_2 alone (Liu et al., 2018) and suggests that other non-CO_2 driving mechanisms (e.g. gateway reorganisation and/or changes in ocean circulation) may influence regional SST patterns.

Of particular relevance is the growing evidence for Northern Component Water (NCW) initiation in the North Atlantic during the early-middle Eocene (~47 to 49 Ma) (Boyle et al., 2017; Hohbein et al., 2012; Norris et al., 2001). The onset of NCW has been attributed to gateway reorganisation, specifically deepening of the Greenland-Scotland Ridge (GSR) (Boyle et al., 2017; Hohbein et al., 2012; Vahlenkamp et al., 2018), although other mechanisms have been proposed such as isolation of the Arctic Ocean (Zhang et al., 2011) or restriction of the Tethys Ocean (Roberts et al., 2009). The onset of NCW is followed by a period of weaker overturning (~42 to 38 Ma) (Witkowski et al., 2021), before re-invigoration of NCW during the late Eocene (∼38 Ma) (Coxall et al., 2018) or Eocene-Oligocene transition (EOT; ∼34 Ma) (Hutchinson et al., 2019). The establishment of NCW can transport additional heat into the eastern North Atlantic (Vahlenkamp et al., 2018), potentially muting any long-term cooling trend in this region. This has been invoked to explain stable temperatures in the eastern North Atlantic during the middle Eocene (Bornemann et al., 2016). However, our understanding of long-term North Atlantic temperature change is based a single proxy record (planktonic foraminiferal $\delta^{18}O$) from a single site (ODP Site 401; Bornemann et al., 2016) and may not be regionally representative.

To test whether the wider North Atlantic region exhibits stable temperatures during the Eocene, we use a multi-proxy approach ($\delta^{18}O$, Mg/Ca, TEX_{86}) to reconstruct SST in the western North Atlantic (Bass River; ODP Leg 174AX; ~36°N paleolatitude) during the early-to-middle Eocene (53.7 to 42.0 Ma). We compare our new dataset with climate model simulations spanning a wide range of CO_2 values to explore (i) temporal and spatial patterns of cooling in the North Atlantic during the Eocene and (ii) whether there is thermal decoupling between the northern and southern hemisphere during the Eocene. This allows us to test whether declining CO_2 is the primary driver of long-term Eocene cooling or whether regional forcing mechanisms are also important.

Methods

Site description

The Bass River section (ODP Leg 174AX; 39°36’N, 74°26’W) consists of calcareous marls and glauconitic silty clays deposited in middle to outer neritic palaeodepths between 30 and 150 m (Fung et al., 2019; Miller et al., 2003). The biostratigraphic age model was developed using planktonic foraminifera and nannofossils (following Fung et al., 2019) with datums converted to the GTS2012 (Vandenberghe et al., 2012).

Analytical methods

Lipid biomarker analysis was performed on 47 sediment samples. Approximately 5-10g of sediment was extracted with an Ethos Ex microwave extraction system using 15 ml of dichloromethane (DCM) and methanol (MeOH) (9:1, *v/v*). The total lipid extract was separated over silica into apolar and polar fractions using hexane:dichloromethane (9:1, *v/v*) and dichloromethane:methanol (1:2, *v/v*), respectively. The polar fraction (containing isoGDGTs) was dissolved in hexane/isopropanol (99:1, *v/v*), passed through 0.45μm PTFE filters and analysed by HPLC/APCI-MS following Hopmans et al. (2016).

Trace element and stable oxygen isotope ($\delta^{18}O$) planktonic foraminiferal analysis was performed on multiple depth intervals (n = 8) spanning the early-to-middle Eocene. Foraminiferal preservation is excellent, appearing transparent or translucent under the light microscope, with no signs of diagenetic alteration observed under SEM (**Figure S1**). Analysis was performed on various surface-dwelling species (*Acarinina praetopilensis, Morozovella formosa, Morozovelloides crassatus, and Pseudohastigerina wilcoxensis*) and deeper, thermocline-dwelling species (*Parasubbotina hagni, Parasubbotina inaequispira*). Single-specimen Mg/Ca analysis was performed via laser ablation-inductively coupled mass spectrometry (LA-ICPMS) (see Müller et al., 2009 and Supplementary Information). Mg/Ca values were determined in multiple chambers (~3 to 5) within a single specimen and averaged. The same specimens were subsequently analysed for

$\delta^{18}O$ using a Multiprep-Isoprime 100 dual inlet system optimised for analysis of single specimens (Supplementary information).

Temperature calibrations

TEX_{86} data was screened using established indices for non-Thaumarchaeota inputs (Supplementary Information; **Figure S5**) and converted to SST using a Bayesian linear calibration (prior mean = 25, prior standard deviation = 10, n = 2000) (Tierney and Tingley, 2014). Planktonic foraminiferal $\delta^{18}O$ values were converted to SST using the bayfox Bayesian calibration (prior mean = 25, prior standard deviation = 20, n = 2000). Seawater $\delta^{18}O$ values ($\delta^{18}O_{sw}$) were defined following the DeepMIP protocols (−1.0‰; see Hollis et al., 2019) with a latitude-specific temporal correction following Gaskell et al. (2022). Data (Meckler et al., 2022) and model-based approaches (Gaskell et al., 2022; Zhu et al., 2020) indicate only minor changes in $\delta^{18}O_{sw}$ at Bass River location through the early-middle Eocene (e.g., <0.05‰ in between x6 and x3 CO_2 simulations using iCESM1.2).

Mg/Ca values were converted to SST using a modified version of MgCaRB (Gray and Evans, 2019) (Supplementary Information). We report pH-corrected Mg/Ca temperatures as the majority of modern foraminifer species are characterised by Mg/Ca-pH sensitivity (Gray and Evans, 2019). For Mg/Ca and $\delta^{18}O$, we report the 'average' SST estimates for a given time slice (n = 8) by combining (i) multiple-specimens from multiple size fractions and (ii) all surface-dwelling species within multiple genera (i.e., *Acarinina praetopilensis, Acarinina pseudotopilensis, Morozovella formosa, Morozovelloides crassatus, Pseudohastigerina wilcoxensis*) into a single estimate, following DeepMIP protocols and adjusting for ODP 174AX sample restrictions (Hollis et al, 2019; Supplementary Information). Average 'SST' estimates comprise a minimum of two samples from a single depth horizon (see **Data S4-S5**). When SSTs are calculated using individual species (**Figure S2**) and size segregating species **(Figure S2-S3**), similar patterns in long-term trends are observed.

Climate model simulations

We use the isotope-enabled Community Earth System Model version 1.2 (iCESM1.2) (Zhu et al., 2020; Zhu et al., 2019) to compare with our proxy reconstructions and to provide an independent estimate of $\delta^{18}O_{sw}$. The iCESM1.2 simulations were performed following the Deep-time Model Intercomparison Project protocols (Lunt et al., 2017) with early Eocene paleogeography and vegetation (56.0–47.8 Ma) (Herold et al., 2014) and atmospheric CO_2 levels of ×1, ×3, ×6, and ×9 preindustrial values (284.7 ppmv). Seawater $\delta^{18}O$ in the simulations was initialized from a constant value of −1.0‰ to account for the absence of ice sheets in a hothouse climate (Hollis et al., 2019). See Zhu et al. (2019; 2020) for further details of the experimental setup, equilibration state, and assessment of the simulation results.

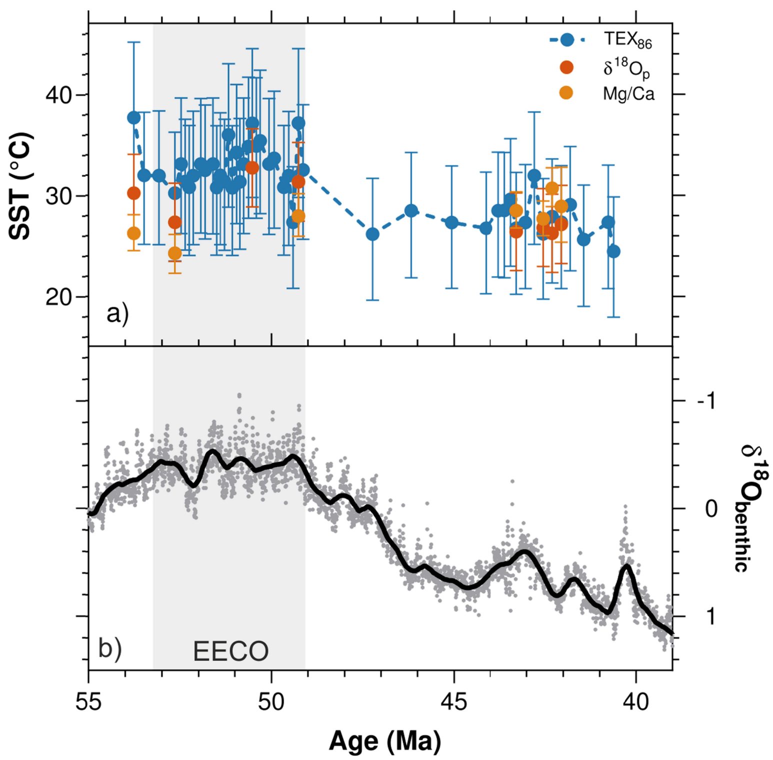

Figure 1. a) SST reconstructions from Bass River during the early-middle Eocene inferred via TEX_{86} (blue), planktonic foraminifera $\delta^{18}O$ (dark orange) and Mg/Ca (light orange). Error bars represent the 95% confidence intervals. Analytical error for $\delta^{18}O$ was better than 0.16 ‰. b) benthic foraminifera $\delta^{18}O$ values (Westerhold et al., 2020).

Results

During the EECO (53.3 to 49.1 Ma), TEX_{86} SST estimates average ~33°C (**Figure 1a**). Between the EECO and the middle Eocene (~40 Ma), TEX_{86} SST estimates decline by ~7°C (**Figure 1a**). Oxygen isotope SST estimates during the EECO from surface-dwelling planktonic foraminiferal average ~30°C (**Figure 1a**). Surface-dwelling species yield higher temperatures (~5 to 6°C) than thermocline-dwelling species but exhibit a similar magnitude of cooling (~3°C) between the EECO and the middle Eocene (~42 Ma) (**Figure S3b**). During the early Eocene, Mg/Ca SST estimates (calculated using the *G. ruber* calibration) average ~26°C (**Figure 1a**). These values are lower than $\delta^{18}O$ and TEX_{86} SST estimates (~30°C and ~33°C, respectively; **Figure 1a**) but agree within the propagated calibration uncertainties. Mg/Ca SST estimates increase by ~3°C between the EECO and middle Eocene (42 Ma; **Figure 1a**). However, the absolute values (~29°C) are comparable to middle Eocene-aged TEX_{86} and $\delta^{18}O$ SST estimates (28°C and 27°C, respectively) and agree within the propagated calibration uncertainties.

Discussion

Long-term cooling in the western North Atlantic during the Eocene

TEX_{86} and $\delta^{18}O$ values indicate very high SSTs at Bass River during the EECO (~30 to 33°C). These values are in agreement with existing low-resolution TEX_{86} estimates generated at Bass River (de Bar et al., 2019) and nearby South Dover Bridge (~34°C; Inglis et al., 2015). Mg/Ca SST estimated are also relatively high (~27°C; **Figure 1**) but are lower than TEX_{86} and $\delta^{18}O$-derived SST estimates by ~3-6°C. Between the EECO and middle Eocene (~43-41 Ma), TEX_{86} and $\delta^{18}O$ values indicate gradual surface water cooling (6 and 3°C, respectively; **Figure 1a**), coherent with declining TEX_{86} SSTs (~7°C) at South Dover Bridge between the EECO and middle Eocene (~42 Ma). Evidence of cooling in multiple proxies and locations provides the first compelling evidence for long-term surface ocean cooling in the (western) North Atlantic between the early and middle Eocene, which is in parallel with the inferred deep-ocean cooling in benthic foraminifera $\delta^{18}O$ record (Figure 1b; Westerhold et al., 2020).

In contrast, our new Mg/Ca SSTs increase by ~3°C between the EECO and middle Eocene. Although middle Eocene (~42 Ma) SST estimates are in excellent agreement with TEX_{86} and $\delta^{18}O$ values **(Figure 1**) and alkenone-derived SST estimates (~29-30°C; Liu et al, 2018) from nearby site IODP Site 1404, the temporal trends are inconsistent with regional observations (*this paper*) (de Bar et al., 2019; Inglis et al., 2015) and declining global bottom water temperature (BWT) estimates inferred via changes in benthic foraminiferal $\delta^{18}O$ values (Figure 1b) (Westerhold et al., 2020).To explore this mismatch further, we compared our proxy-derived temperature estimates (TEX_{86}, Mg/Ca, $\delta^{18}O$) alongside iCESM1.2 simulations with different CO_2 scenarios (x1 to x9 pre-industrial CO_2) (**Figure 2**). These simulations have previously been shown to replicate key large-scale features of the early Eocene including enhanced global mean surface temperature estimates (Lunt et al., 2021; Zhu et al., 2019), reduced meridional temperature gradients (Lunt et al., 2021), changes in the hydrological cycle (Cramwinckel et al., 2022), and the values and distribution of planktonic foraminifera $\delta^{18}O$ values (Zhu et al., 2020). iCESM1.2 simulated SST at the Bass River is 30.7 and 26.6 ℃ in the ×6 and ×3 PI CO_2 simulations, respectively, which overlaps with proxy reconstructions (Figure 2). For a two-fold decrease in atmospheric CO_2 (i.e., from ×6 to ×3 PI CO_2), the model predicted decrease in SST of ~4°C is comparable to the magnitude of cooling captured by TEX_{86} and $\delta^{18}O$ (6 and 3 °C, respectively; **Figure 2**) between the EECO and middle Eocene, but is inconsistent with warming observed in Mg/Ca values. Given that proxy-derived CO_2 estimates declines from ~1470 ppm (~×5 PI CO_2) to ~800ppm (~×3 PI CO_2) during this interval (Anagnostou et al., 2020), this implies additional non-thermal controls on Mg/Ca values at this site.

The choice of Mg/Ca calibration remains uncertain when working with extinct species. However, the discrepancy between Mg/Ca-derived SSTs and other proxy data is insensitive to the choice of Mg/Ca calibration approach (see Supplementary Information). This is because seawater pH was substantially lower than modern throughout the Eocene (Anagnostou et al., 2020), such that choosing a *G. ruber* or *T. sacculifer*-like calibration has a minor effect on the long-term Mg/Ca-derived trend in our dataset (**Figure S4**). Seawater Mg/Ca is also well-constrained for the Eocene

(Evans et al., 2018; Gothmann et al., 2015) and is broadly invariant across this interval, such that it is very unlikely that unidentified changes mask cooling. Given that this site was targeted for its exceptional foraminiferal preservation and diverse assemblages (**Figure S1),** this potentially points towards either an evolutionary control on Eocene planktonic foraminifera Mg incorporation, or a shift in seawater carbonate chemistry at this site that substantially differs from the existing pH records (Anagnostou et al., 2020; Rae et al., 2021; see Supplementary Information for more discussion). Resolving this issue and exploring any other additional controls (e.g., local hydrographic variability; c.f. Thornalley et al., 2011) will require further data and is beyond the scope of this study. However, we continue to include the Mg/Ca SST estimates in our assessment of the thermal evolution of the North Atlantic. We also note that this discrepancy may ultimately stem from a small number of Mg/Ca analyses (n=7) from two time slices in the early Eocene (Figure 2), such that this may simply highlight the benefit of working with larger numbers of specimens, where possible.

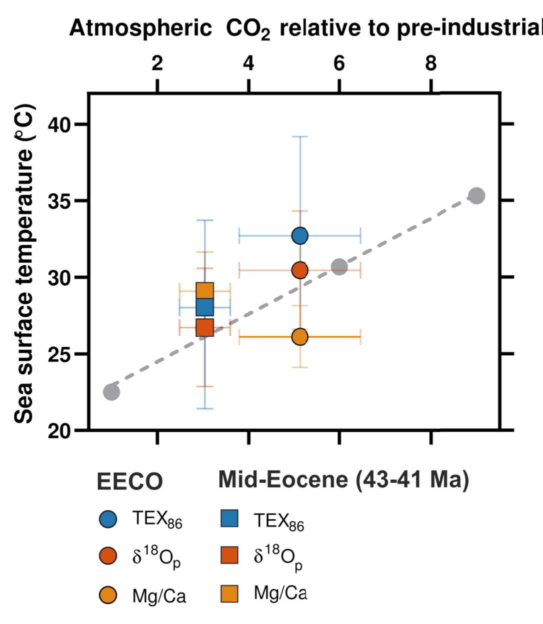

Figure 2: Data-model comparison for Bass River. Grey circles show the CO_2 concentration and sea surface temperature (SST) in the iCESM1.2 simulations (this paper; Zhu et al., 2019).

Dashed line represents a simple linear regression through the model output. Coloured symbols show proxy SST estimates (*this paper*) and CO_2 (Anagnostou et al., 2020) for the EECO (53.3-49.1 Ma; coloured circles) and middle Eocene (43-41 Ma; coloured squares). Error bars represent 90% confidence intervals (SST) or ± 2 standard deviations (CO_2).

Divergent zonal temperature gradients in the North Atlantic during the early-to-middle Eocene

Overall, our new multi-proxy (TEX86, $\delta^{18}O$, Mg/Ca) results indicate net cooling (~4°C) in the western North Atlantic between the EECO and middle Eocene (**Figure 1**). Our data from the western North Atlantic contrasts with existing planktonic foraminifera $\delta^{18}O$-derived SST estimates from the eastern North Atlantic (~37° N; ODP Site 401; Bornemann et al., 2016) that indicate minimal (<1°C) or no cooling between the EECO (ca. 49-50 Ma) and late middle Eocene (ca. 40 – 42 Ma) (**Figure 3a**). The lack of cooling at ODP Site 401 would not be expected from a long-term decline in atmospheric CO_2. Furthermore, the east-west zonal mean temperature gradient inferred via proxy estimates (~15-20°C) is much larger than inferred via model simulations (~2~3°C; **Figure 3b**) with a range of plausible CO_2 (x1 to x9 pre-industrial CO_2). Collectively, this strongly implies that other factors influence SSTs in the eastern North Atlantic (ODP Site 401; Bornemann et al., 2016) during the Eocene.

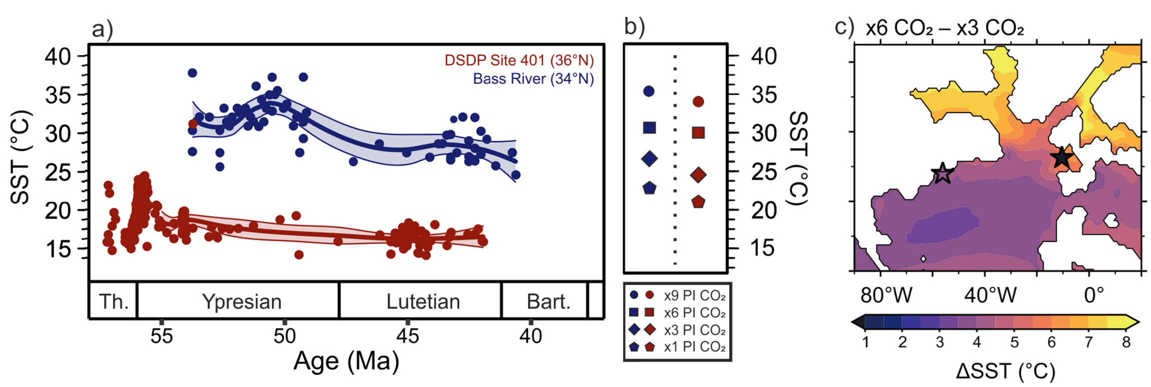

Figure 3: Divergent zonal temperature gradients in the North Atlantic during the early-to-middle Eocene. a) proxy-derived SST reconstructions for Bass River (*this study*) and ODP Site 401 ($\delta^{18}O$ only) (Bornemann et al, 2016) fitted with a LOESS regression. $\delta^{18}O$ values from ODP Site 401 re-

calculated for surface-dwelling foraminiferal genera (*Acarinina and Morozovella* spp.) using the bayfox Bayesian calibration ($\delta^{18}O_{sw}$ = -1.0, prior mean = 25, prior standard deviation = 20, n = 2000). Error bars represent the 95% confidence intervals. b) iCESM1.2-derived SST estimates for Bass River (blue symbols) and ODP Site 401 (red symbols) under different CO_2 concentrations, c) iCESM1.2-derived ΔSST estimates (x6 PI CO_2 - x3 PI CO_2) with proxy-derived cooling between the early- to middle Eocene shown for each site.

Planktonic foraminifera at Bass River exhibit excellent preservation (Supplementary Information) and tests are translucent and 'glassy' (**Figure S1**), whereas post-PETM aged planktonic foraminifera at ODP Site 401 exhibit relatively poor preservation (Bornemann et al., 2016) and have been classified as 'recrystallized' (see Hollis al. 2019). However, the influence of diagenesis would act to increase $\delta^{18}O$ values and overestimate (rather than underestimate) the magnitude of cooling. Therefore, this is unlikely to explain the observed trends (Figure 3). Alternatively, changes in ocean circulation could have modulated regional temperature patterns in the eastern North Atlantic during the middle-to-late Eocene. Recent idealised modelling experiments show that deepening of the Greenland-Scotland Ridge can initiate Northern Component Water (NCW) formation in the North Atlantic and increase SST in the eastern North Atlantic by up to 7 °C (Vahlenkamp et al., 2018) and could have muted any long-term CO_2-driven cooling at ODP Site 401. In contrast, deepening of the Greenland-Scotland Ridge has only a minimal influence (< 1°C) on SSTs in the western North Atlantic (i.e., where Bass River is located) (Vahlenkamp et al., 2018).

There is growing geochemical and sedimentological evidence placing the initial onset of NCW between ~47 and 49 Ma, coincident with changes in zonal temperature gradients between the eastern and western North Atlantic. Evidence for early onset of NCW between ~47 and 49 Ma includes development of contourite drifts in the western North Atlantic (Boyle et al., 2017), changes in biosiliceous sedimentation (Witkowski et al., 2021) and a collapse in $\delta^{13}C$ gradients between the North and South Atlantic (Hohbein et al., 2012). These changes would also influence local hydrography within the eastern North Atlantic and could exert an additional control on $\delta^{18}O_{sw}$

values at ODP Site 401. Proxy-based reconstructions during the Middle Eocene Climatic Optimum; have argued that northward expansion of the North Atlantic subtropical gyre could also act as a mechanism to increase SSTs within the North Atlantic (Van Der Ploeg et al., 2023). However, these large-scale regional patterns are not evident in Eocene model simulations and additional proxy data is required to test this further. Thus, we argue that (i) tectonic gateways and changes in ocean circulation may exert a local control on spatial patterns of cooling temperatures, especially in the North Atlantic during the early-to-middle Eocene, and (ii) that diverging zonal temperature gradients in the North Atlantic are consistent with the initial early onset of NCW.

Synchronous surface water cooling in the northern and southern hemispheres during the Eocene

Our new multi-proxy SST estimates (**Figure 1)** provide evidence for long-term cooling in the (western) North Atlantic during the middle Eocene. To explore whether long-term cooling is globally synchronous, we compiled early and middle Eocene (56 to 38 Ma) SST estimates from three key regions: (i) the equatorial Atlantic (0-30° N/S) (Cramwinckel et al., 2018; Zhang et al., 2013; Inglis et al., 2015), (ii) the Northwest Atlantic (30-50 °N) (*this study*; de Bar et al., 2019; Inglis et al., 2015; Liu et al., 2018; van der Ploeg et al., 2023) and (iii) the SW Pacific (>50°S) (Bijl et al., 2013; Bijl et al., 2009; Crouch et al., 2020; Hollis et al., 2009; Inglis et al., 2015). (**Figure 4;** see also Supplementary Information).

Our results show that the onset of long-term cooling (i.e., post EECO) occurs synchronously around 50-49 Ma in the North Atlantic and SW Pacific (i.e. towards the termination of the EECO; **Figure 4a-c**) and coincides with an increase in the latitudinal SST gradient **(Figure 4d**). This illustrates that the onset of Eocene cooling is a globally feature and consistent with a decline in atmospheric CO_2 as a forcing mechanism for cooling. During the middle Eocene (~47-42 Ma), there is a gradual decrease in the latitudinal SST gradient between the equatorial Atlantic and North Atlantic **(Figure 4d)**, implying that NCW formation may have also masked long-term CO_2-driven cooling in the eastern North Atlantic. This can be tested by developing new long-term SSTs records from other regions in the subpolar North Atlantic that could be sensitive to NCW formation (e.g., the Nordic Sea). Alternatively, the magnitude of cooling in the equatorial Atlantic could be exaggerated. Indeed, ODP Site 959 (located in the eastern equatorial Atlantic) is unlikely to be representative of the global tropical ocean signal, because it is located in an area of upwelling, thus physically linked to subsurface waters. There is also evidence for an increase in upwelling during the middle-to-late Eocene at ODP Site 959 which could lead to lower-than-expected SSTs (Cramwinckel et al., 2018).

There is also a dramatic decrease in SW Pacific SST estimates ~46-47 Ma (**Figure 4**c) and strengthening of the low-to-high latitude temperature gradient (**Figure 4d**) that is not reflected in either the low- or mid-latitude Atlantic (**Figure 4d**), suggesting additional non-CO_2 controls in the SW Pacific. Previous work argues that the Tasman Gateway was open to shallow circulation at this time (~49 to 46 Ma) (Bijl et al., 2013) and deepening of the Tasman Gateway would initiate regional surface water cooling (Sijp et al., 2011; Sijp et al., 2016) and may account for declining SSTs. Our study reveals that changes in ocean gateways may have influenced spatial patterns of cooling in the North Atlantic (see above) and perhaps also in the SW Pacific (Sijp et al., 2016), but that CO_2 was likely responsible for the majority of long-term Eocene cooling.

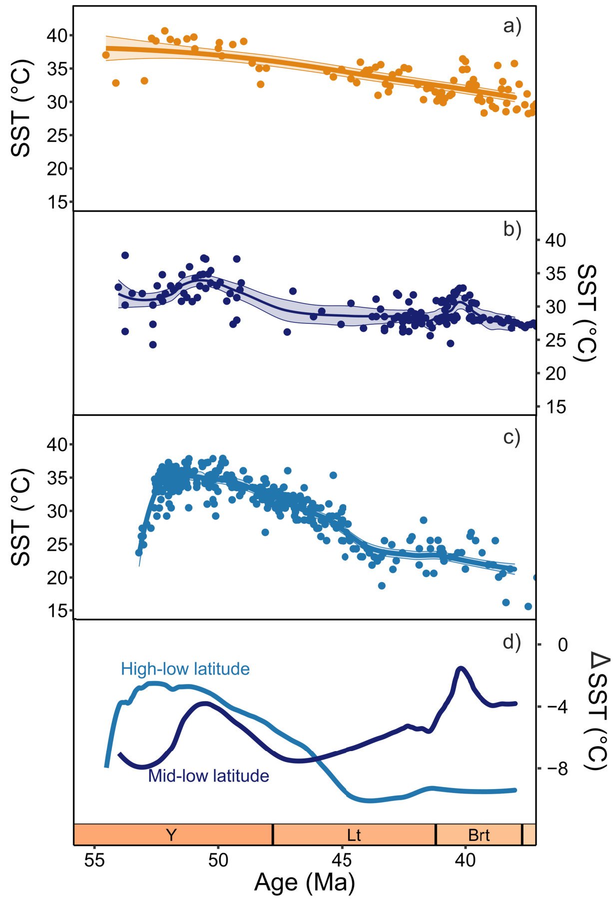

Figure 4: Long-term evolution of surface ocean temperatures during the Eocene in the (a) equatorial Atlantic (Cramwinckel et al., 2018; Inglis et al., 2015; Zhang et al., 2013), b) North Atlantic (this study; Inglis et al., 2015; de Bar et al., 2019), and c) the SW Pacific (Bijl et al., 2013; Bijl et al., 2009; Crouch et al., 2020; Hollis et al., 2009; Inglis et al., 2015). Panel (d) shows the SST gradient between the equatorial Atlantic and the North Atlantic (dark blue line) and SW Pacific (light blue line). To determine the long-term mean SST evolution for the low-, mid-, and high-latitudes, nonparametric LOESS regressions were fitted using the fANCOVA software package (http://www.R-project.org/).

4 Conclusions

Here we present the first multi-proxy (Mg/Ca, $\delta^{18}O$, TEX_{86}) SST record from the western North Atlantic spanning the early-to-middle Eocene. Our results reconstruct very high SSTs during the early Eocene Climatic Optimum (~27-33°C), in agreement with high atmospheric CO_2 concentrations. Our multi-proxy results indicate a slow decline (~5°C) in SSTs between the early (~53 Ma) and the middle Eocene (~42 Ma), consistent with long-term decrease in atmospheric CO_2. However, zonal temperature gradients in the North Atlantic are likely decoupled during the early-to-middle Eocene. We attribute this to the inception of Northern Component Water at the early-middle Eocene transition and incursion of warmer waters into the eastern North Atlantic. We demonstrate that the onset of long-term Eocene cooling in the western North Atlantic (~50-49 Ma) occurs synchronously in other ocean basins (e.g., N. Atlantic vs S. Pacific) and across different latitudinal bands. This indicates that CO_2 was likely responsible for the onset of long-term Eocene cooling, but that changes in ocean gateways likely influenced spatial patterns of cooling in different ocean basins, especially during the middle Eocene.

Acknowledgements

Samples were provided by IODP which is sponsored by the NSF and participating countries. We thank Jim Browning for information on the age model and Tianchen He for support in trace element and isotope data interpretation. GNI was supported by a Royal Society Dorothy Hodgkin Fellowship (DHF\R1\191178) and NERC (NE/V018388/1). We thank NEIF-B for analytical support and Jim Davy for support with SEM imaging. RB acknowledges funding from a NERC PhD studentship award number 1352360, the Cushman Foundation for Foraminiferal Research (Joseph A. Cushman Award for Student Research), and a 2016 Geologists' Association New Researchers' Award. BW was supported by NERC grants NE/V018361/1 and NE/G014817. LA-ICPMS work at Royal Holloway University of London was partly funded by a 2014 NERC Capital Equipment Grant (Ref: CC073). The CESM project is supported primarily by the National Science Foundation (NSF). This material is based upon work supported by the National Center for Atmospheric Research, which is a major facility sponsored by the NSF under Cooperative Agreement No. 1852977. JZ was supported by NSF Grant 2202777.

Open Research

Inorganic and organic geochemical data is available in the supporting information and at OSF (DOI pending).

References

Anagnostou, E., John, E. H., Babila, T., Sexton, P., Ridgwell, A., Lunt, D. J., Pearson, P. N., Chalk, T., Pancost, R. D., and Foster, G., 2020, Proxy evidence for state-dependence of climate sensitivity in the Eocene greenhouse: Nature Communications, v. 11, no. 1, p. 1-9.

Barker, S., Cacho, I., Benway, H., and Tachikawa, K., 2005, Planktonic foraminiferal Mg/Ca as a proxy for past oceanic temperatures: a methodological overview and data compilation for the Last Glacial Maximum: Quaternary Science Reviews, v. 24, no. 7-9, p. 821-834.

Bijl, P. K., Bendle, J. A. P., Bohaty, S. M., Pross, J., Schouten, S., Tauxe, L., Stickley, C. E., McKay, R. M., Röhl, U., Olney, M., Sluijs, A., Escutia, C., Brinkhuis, H., and Scientists, E., 2013, Eocene cooling linked to early flow across the Tasmanian Gateway: Proceedings of the National Academy of Sciences, v. 110, no. 24, p. 9645-9650.

Bijl, P. K., Schouten, S., Sluijs, A., Reichart, G.-J., Zachos, J. C., and Brinkhuis, H., 2009, Early Palaeogene temperature evolution of the southwest Pacific Ocean: Nature, v. 461, no. 7265, p. 776-779.

Bornemann, A., D'haenens, S., Norris, R. D., and Speijer, R. P., 2016, The demise of the early Eocene greenhouse–Decoupled deep and surface water cooling in the eastern North Atlantic: Global and Planetary Change, v. 145, p. 130-140.

Bornemann, A., Norris, R. D., Lyman, J. A., D'Haenens, S., Groeneveld, J., Röhl, U., Farley, K. A., and Speijer, R. P., 2014, Persistent environmental change after the Paleocene–Eocene Thermal Maximum in the eastern North Atlantic: Earth and Planetary Science Letters, v. 394, p. 70-81.

Boyle, P. R., Romans, B. W., Tucholke, B. E., Norris, R. D., Swift, S. A., and Sexton, P. F., 2017, Cenozoic North Atlantic deep circulation history recorded in contourite drifts, offshore Newfoundland, Canada: Marine Geology, v. 385, p. 185-203.

Coxall, H. K., Huck, C. E., Huber, M., Lear, C. H., Legarda-Lisarri, A., O'regan, M., Sliwinska, K. K., Van De Flierdt, T., De Boer, A. M., and Zachos, J. C., 2018, Export of nutrient rich Northern Component Water preceded early Oligocene Antarctic glaciation: Nature Geoscience, v. 11, no. 3, p. 190-196.

Cramwinckel, M. J., Huber, M., Kocken, I. J., Agnini, C., Bijl, P. K., Bohaty, S. M., Frieling, J., Goldner, A., Hilgen, F. J., and Kip, E. L., 2018, Synchronous tropical and polar temperature evolution in the Eocene: Nature, v. 559, no. 7714, p. 382-386.

Crouch, E., Shepherd, C., Morgans, H., Naafs, B., Dallanave, E., Phillips, A., Hollis, C., and Pancost, R. D., 2020, Climatic and environmental changes across the early Eocene climatic optimum at mid-Waipara River, Canterbury Basin, New Zealand: Earth-Science Reviews, v. 200, p. 102961.

de Bar, M., de Nooijer, L., Schouten, S., Ziegler, M., Sluijs, A., and Reichart, G. J., 2019, Comparing seawater temperature proxy records for the past 90 Myrs from the shallow shelf record Bass River, New Jersey: Paleoceanography and Paleoclimatology, v. 34, no. 4, p. 455-475.

Evans, D., Sagoo, N., Renema, W., Cotton, L. J., Müller, W., Todd, J. A., Saraswati, P. K., Stassen, P., Ziegler, M., and Pearson, P. N., 2018, Eocene greenhouse climate revealed by coupled clumped isotope-Mg/Ca thermometry: Proceedings of the National Academy of Sciences, v. 115, no. 6, p. 1174-1179.

Fung, M. K., Katz, M. E., Miller, K. G., Browning, J. V., and Rosenthal, Y., 2019, Sequence stratigraphy, micropaleontology, and foraminiferal geochemistry, Bass River, New Jersey paleoshelf, USA: Implications for Eocene ice-volume changes: Geosphere, v. 15, no. 2, p. 502-532.

Gaskell, D. E., Huber, M., O'Brien, C. L., Inglis, G. N., Acosta, R. P., Poulsen, C. J., and Hull, P. M., 2022, The latitudinal temperature gradient and its climate dependence as inferred from foraminiferal δ18O over the past 95 million years: Proceedings of the National Academy of Sciences, v. 119, no. 11, p. e2111332119.

Gothmann, A. M., Stolarski, J., Adkins, J. F., Schoene, B., Dennis, K. J., Schrag, D. P., Mazur, M., and Bender, M. L., 2015, Fossil corals as an archive of secular variations in seawater chemistry since the Mesozoic: Geochimica et Cosmochimica Acta, v. 160, p. 188-208.

Gray, W. R., and Evans, D., 2019, Nonthermal influences on Mg/Ca in planktonic foraminifera: A review of culture studies and application to the last glacial maximum: Paleoceanography and Paleoclimatology, v. 34, no. 3, p. 306-315.

Herold, N., Buzan, J., Seton, M., Goldner, A., Green, J., Müller, R., Markwick, P., and Huber, M., 2014, A suite of early Eocene (~ 55 Ma) climate model boundary conditions: Geoscientific Model Development.

Hohbein, M. W., Sexton, P. F., and Cartwright, J. A., 2012, Onset of North Atlantic Deep Water production coincident with inception of the Cenozoic global cooling trend: Geology, v. 40, no. 3, p. 255-258.

Hollis, C. J., Dunkley Jones, T., Anagnostou, E., Bijl, P. K., Cramwinckel, M. J., Cui, Y., Dickens, G. R., Edgar, K. M., Eley, Y., and Evans, D., 2019a, The DeepMIP contribution to PMIP4: methodologies for selection, compilation and analysis of latest Paleocene and early Eocene climate proxy data, incorporating version 0.1 of the DeepMIP database: Geoscientific Model Development, v. 12, no. 7, p. 3149-3206.

Hollis, C. J., Dunkley Jones, T., Anagnostou, E., Bijl, P. K., Cramwinckel, M. J., Cui, Y., Dickens, G. R., Edgar, K. M., Eley, Y., Evans, D., Foster, G. L., Frieling, J., Inglis, G. N., Kennedy, E. M., Kozdon, R., Lauretano, V., Lear, C. H., Littler, K., Lourens, L., Meckler, A. N., Naafs, B. D. A., Pälike, H., Pancost, R. D., Pearson, P. N., Röhl, U., Royer, D. L., Salzmann, U., Schubert, B. A., Seebeck, H., Sluijs, A., Speijer, R. P., Stassen, P., Tierney, J., Tripati, A., Wade, B., Westerhold, T., Witkowski, C., Zachos, J. C., Zhang, Y. G., Huber, M., and Lunt, D. J., 2019b, The DeepMIP contribution to PMIP4: methodologies for selection, compilation and analysis of latest Paleocene and early Eocene climate proxy data, incorporating version 0.1 of the DeepMIP database: Geosci. Model Dev., v. 12, no. 7, p. 3149-3206.

Hollis, C. J., Handley, L., Crouch, E. M., Morgans, H. E., Baker, J. A., Creech, J., Collins, K. S., Gibbs, S. J., Huber, M., and Schouten, S., 2009, Tropical sea temperatures in the high-latitude South Pacific during the Eocene: Geology, v. 37, no. 2, p. 99-102.

Hollis, C. J., Taylor, K. W. R., Handley, L., Pancost, R. D., Huber, M., Creech, J. B., Hines, B. R., Crouch, E. M., Morgans, H. E. G., Crampton, J. S., Gibbs, S., Pearson, P. N., and Zachos, J. C., 2012, Early Paleogene temperature history of the Southwest Pacific Ocean: Reconciling proxies and models: Earth and Planetary Science Letters, v. 349–350, no. 0, p. 53-66.

Hopmans, E. C., Schouten, S., and Damsté, J. S. S., 2016, The effect of improved chromatography on GDGT-based palaeoproxies: Organic Geochemistry, v. 93, p. 1-6.

Hutchinson, D. K., Coxall, H. K., O'Regan, M., Nilsson, J., Caballero, R., and de Boer, A. M., 2019, Arctic closure as a trigger for Atlantic overturning at the Eocene-Oligocene Transition: Nature Communications, v. 10, no. 1, p. 3797.

Inglis, G. N., Farnsworth, A., Lunt, D., Foster, G. L., Hollis, C. J., Pagani, M., Jardine, P. E., Pearson, P. N., Markwick, P., Galsworthy, A. M. J., Raynham, L., Taylor, K. W. R., and Pancost, R. D., 2015, Descent toward the icehouse; Eocene sea surface cooling inferred from GDGT distributions: Paleoceanography, v. 30, no. 7, p. 1000.

Inglis, G. N., and Tierney, J. E., 2020, The TEX86 Paleotemperature Proxy, Cambridge University Press.

Liu, Z., He, Y., Jiang, Y., Wang, H., Liu, W., Bohaty, S. M., and Wilson, P. A., 2018, Transient temperature asymmetry between hemispheres in the Palaeogene Atlantic Ocean: Nature Geoscience, v. 11, no. 9, p. 656-660.

Lunt, D. J., Bragg, F., Chan, W.-L., Hutchinson, D. K., Ladant, J.-B., Morozova, P., Niezgodzki, I., Steinig, S., Zhang, Z., and Zhu, J., 2021, DeepMIP: Model intercomparison of early Eocene climatic optimum (EECO) large-scale climate features and comparison with proxy data: Climate of the Past, v. 17, no. 1, p. 203-227.

Lunt, D. J., Huber, M., Anagnostou, E., Baatsen, M. L., Caballero, R., DeConto, R., Dijkstra, H. A., Donnadieu, Y., Evans, D., and Feng, R., 2017, The DeepMIP contribution to PMIP4:

Experimental design for model simulations of the EECO, PETM, and pre-PETM (version 1.0): Geoscientific Model Development, v. 10, no. 2, p. 889-901.

Meckler, A. N., Sexton, P., Piasecki, A., Leutert, T., Marquardt, J., Ziegler, M., Agterhuis, T., Lourens, L., Rae, J., and Barnet, J., 2022, Cenozoic evolution of deep ocean temperature from clumped isotope thermometry: Science, v. 377, no. 6601, p. 86-90.

Miller, K., Sugarman, P., and Browning, J., 1. BASS RIVER SITE1.

Miller, K. G., Browning, J. V., Sugarman, P. J., McLaughlin, P. P., Kominz, M. A., Olsson, R. K., Wright, J. D., Cramer, B. S., Pekar, S., and Van Sickel, W., 2003, 174AX leg summary: Sequences, sea level, tectonics, and aquifer resources: Coastal plain drilling: Proceedings of Ocean Drilling Program, Initial Reports, 174AX (Suppl.)(Ed. by KG Miller, PJ Sugarman & JV Browning, et al.) pp, p. 1-40.

Müller, W., Shelley, M., Miller, P., and Broude, S., 2009, Initial performance metrics of a new custom-designed ArF excimer LA-ICPMS system coupled to a two-volume laser-ablation cell: Journal of Analytical Atomic Spectrometry, v. 24, no. 2, p. 209-214.

Norris, R., Klaus, A., and Kroon, D., 2001, Mid-Eocene deep water, the late Palaeocene thermal maximum and continental slope mass wasting during the Cretaceous-Palaeogene impact: Geological Society, London, Special Publications, v. 183, no. 1, p. 23-48.

Roberts, C. D., LeGrande, A. N., and Tripati, A. K., 2009, Climate sensitivity to Arctic seaway restriction during the early Paleogene: Earth and Planetary Science Letters, v. 286, no. 3-4, p. 576-585.

Sijp, W. P., England, M. H., and Huber, M., 2011, Effect of the deepening of the Tasman Gateway on the global ocean: Paleoceanography, v. 26, no. 4.

Sijp, W. P., von der Heydt, A. S., and Bijl, P. K., 2016, Model simulations of early westward flow across the Tasman Gateway during the early Eocene: Climate of the Past, v. 12, no. 4, p. 807-817.

Tierney, J. E., and Tingley, M. P., 2014, A Bayesian, spatially-varying calibration model for the TEX< sub> 86</sub> proxy: Geochimica et Cosmochimica Acta, v. 127, p. 83-106.

Vahlenkamp, M., Niezgodzki, I., De Vleeschouwer, D., Lohmann, G., Bickert, T., and Pälike, H., 2018, Ocean and climate response to North Atlantic seaway changes at the onset of long-term Eocene cooling: Earth and Planetary Science Letters, v. 498, p. 185-195.

Van Der Ploeg, R., Cramwinckel, M. J., Kocken, I. J., Leutert, T. J., Bohaty, S. M., Fokkema, C. D., Hull, P. M., Meckler, A. N., Middelburg, J. J., and Müller, I. A., 2023, North Atlantic surface ocean warming and salinization in response to middle Eocene greenhouse warming: Science advances, v. 9, no. 4, p. eabq0110.

Westerhold, T., Marwan, N., Drury, A. J., Liebrand, D., Agnini, C., Anagnostou, E., Barnet, J. S., Bohaty, S. M., De Vleeschouwer, D., and Florindo, F., 2020, An astronomically dated record of Earth's climate and its predictability over the last 66 million years: Science, v. 369, no. 6509, p. 1383-1387.

Witkowski, J., Bryłka, K., Bohaty, S. M., Mydłowska, E., Penman, D. E., and Wade, B. S., 2021, North Atlantic marine biogenic silica accumulation through the early to middle Paleogene: implications for ocean circulation and silicate weathering feedback: Climate of the Past, v. 17, no. 5, p. 1937-1954.

Zhang, Y. G., Pagani, M., Liu, Z., Bohaty, S. M., and DeConto, R., 2013, A 40-million-year history of atmospheric CO2: Philosophical Transactions of the Royal Society A: Mathematical, Physical and Engineering Sciences, v. 371, no. 2001.

Zhang, Z., Nisancioglu, K. H., Flatøy, F., Bentsen, M., Bethke, I., and Wang, H., 2011, Tropical seaways played a more important role than high latitude seaways in Cenozoic cooling: Climate of the Past, v. 7, no. 3, p. 801-813.

Zhu, J., Poulsen, C. J., Otto-Bliesner, B. L., Liu, Z., Brady, E. C., and Noone, D. C., 2020, Simulation of early Eocene water isotopes using an Earth system model and its implication for past climate reconstruction: Earth and Planetary Science Letters, v. 537, p. 116164.

Zhu, J., Poulsen, C. J., and Tierney, J. E., 2019, Simulation of Eocene extreme warmth and high climate sensitivity through cloud feedbacks: Science Advances, v. 5, no. 9, p. eaax1874.

Figure 1.

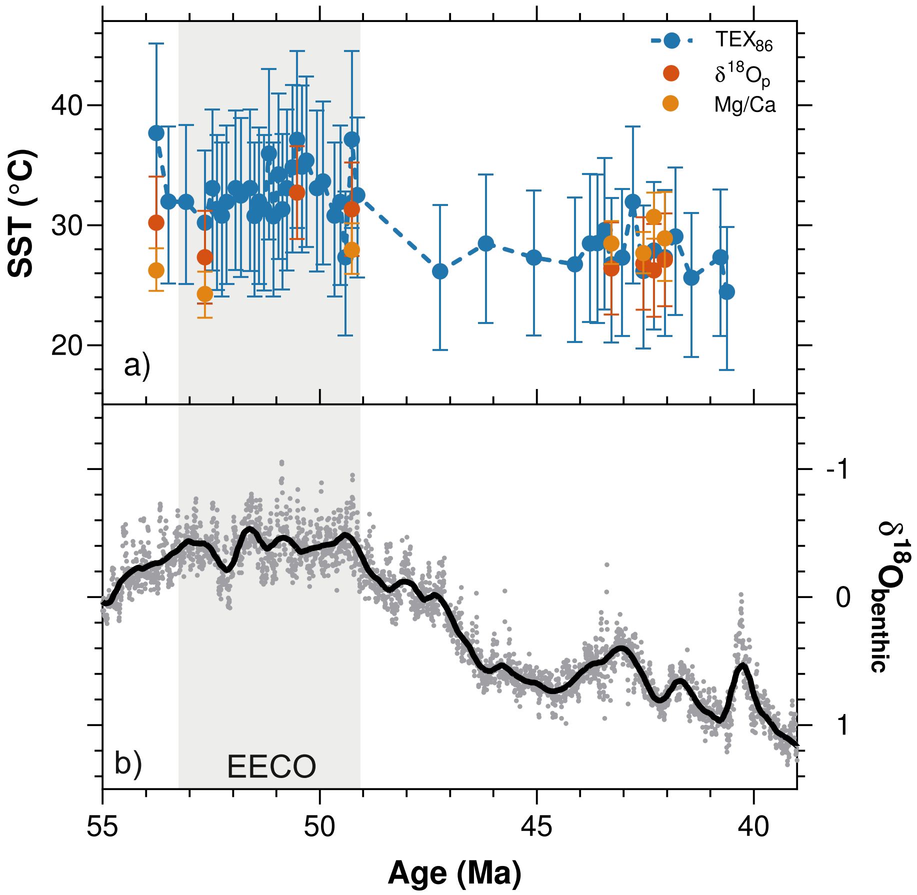

TEX86
δ18Op
Mg/Ca
SST (°C)
40
30
20
a)
b)
EECO
-1
0
1
δ18Obenthic
55
50
45
40
Age (Ma)

Figure 2.

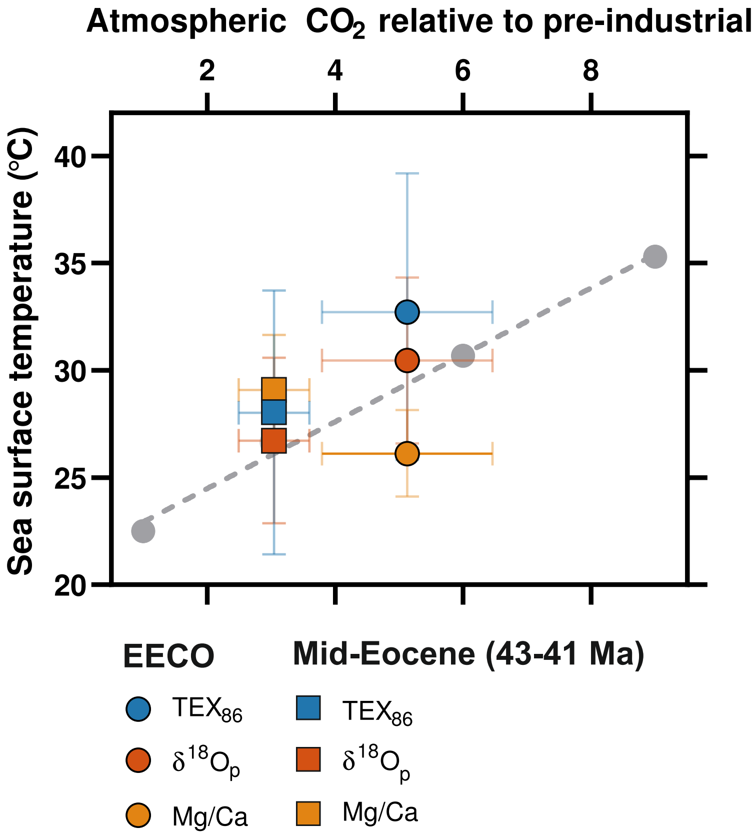

Atmospheric CO_2 relative to pre-industrial
2
4
6
8
Sea surface temperature (°C)
40
35
30
25
20
EECO
TEX86
δ18Op
Mg/Ca
Mid-Eocene (43-41 Ma)
TEX86
δ18Op
Mg/Ca

Figure 3.

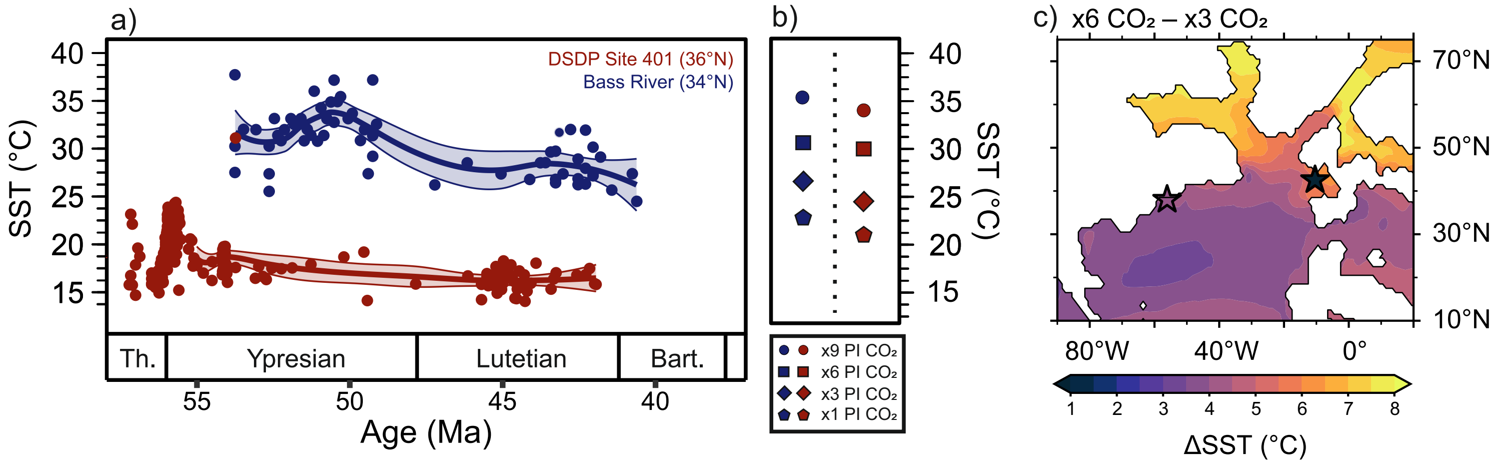
a)
DSDP Site 401 (36°N)
Bass River (34°N)
SST (°C)
Th.
Ypresian
Lutetian
Bart.
Age (Ma)
b)
SST (°C)
x9 PI CO₂
x6 PI CO₂
x3 PI CO₂
x1 PI CO₂
c) x6 CO₂ – x3 CO₂
70°N
50°N
30°N
10°N
80°W
40°W
0°
ΔSST (°C)

Figure 4.

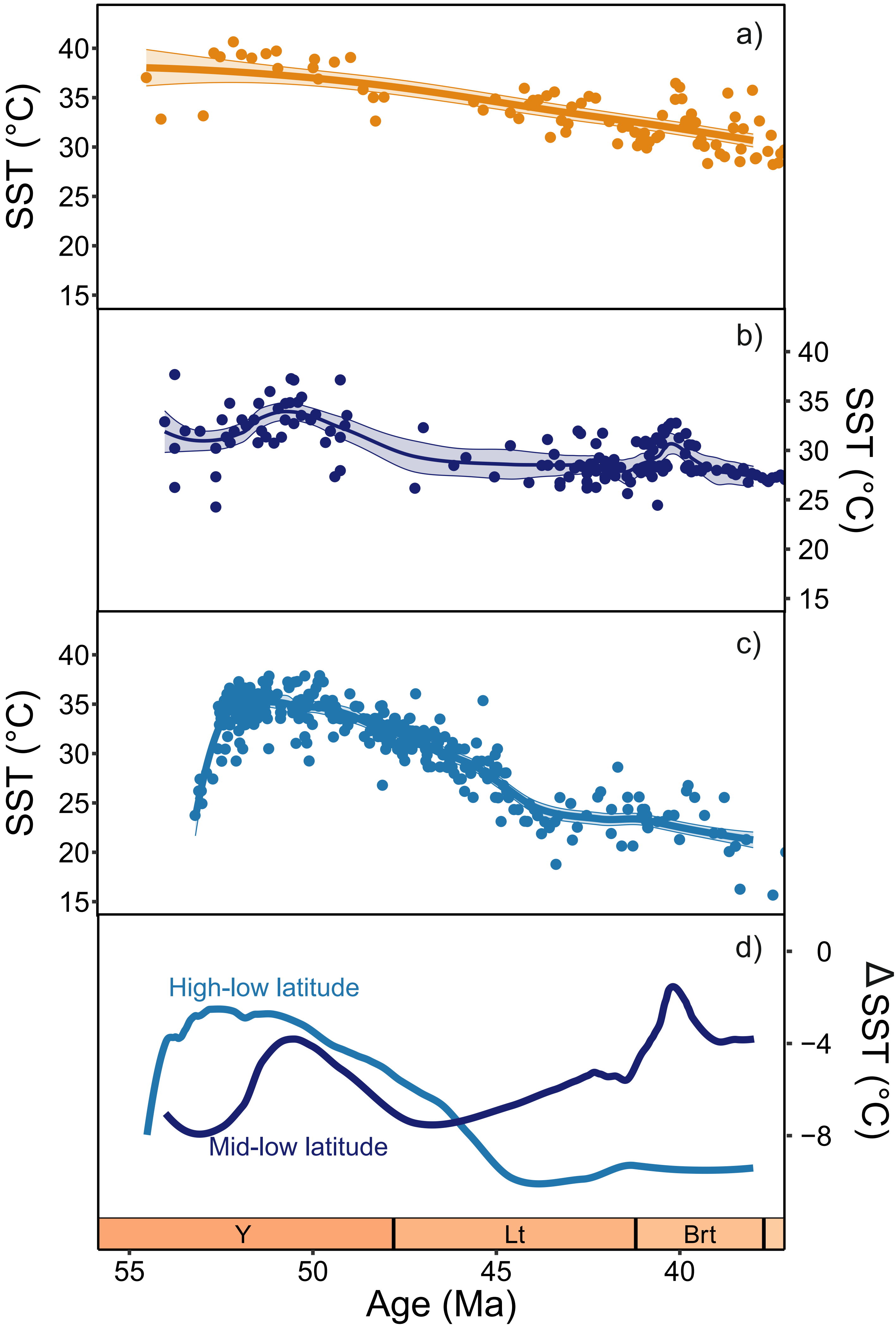
a)
b)
c)
d)
SST (°C)
40
35
30
25
20
15
ΔSST (°C)
0
−4
−8
High-low latitude
Mid-low latitude
Y
Lt
Brt
55
50
45
40
Age (Ma)